Reaction mechanism of core–shell MoO_2/MoS_2 nanoflakes via plasma-assisted sulfurization of MoO_3

2016 Mater. Res. Express 3 055021

(http://iopscience.iop.org/2053-1591/3/5/055021)

Materials Research Express

RECEIVED
2 April 2016

REVISED
2 May 2016

ACCEPTED FOR PUBLICATION
6 May 2016

PUBLISHED
19 May 2016

PAPER

Reaction mechanism of core–shell MoO_2/MoS_2 nanoflakes via plasma-assisted sulfurization of MoO_3

Prabhat Kumar, Megha Singh, Rabindar K Sharma and G B Reddy

Thin film laboratory, Department of Physics, Indian Institute of Technology Delhi, New Delhi, India-110016

E-mail: prabhat89k@gmail.com

Keywords: plasma-assisted sulfurization, core–shell, nanoflakes, thin films and interfaces

Abstract

The sulfurization of MoO_3 in an H_2S/Ar plasma atmosphere has been experimentally studied and a reaction mechanism has been proposed based on the results obtained. Nanostructured thin films (NTFs) of MoO_3 were sulfurized at different temperatures varying from 150 °C to 550 °C. High-resolution transmission electron microscopy (TEM) images depict core–shell nanoflakes with varying shell thicknesses as the sulfurization temperature (T_{sn}) is varied. The shells consist of MoS_2 and the core is MoO_2/MoO_3. X-ray diffraction (XRD) and Raman analysis have been used to study the structural changes as MoO_3 is sulfurized. The analyses showed two phases, MoO_2 and MoS_2, at low temperatures ($\leqslant$350 °C), whereas the films sulfurized at higher temperatures show predominantly MoS_2. The scanning electron microscopy (SEM) results show no noticeable changes in the surface morphology of the NTFs after sulfurization. X-ray photoelectron spectroscopy (XPS) was carried out to calculate the relative percentages of MoO_3, MoO_2 and MoS_2. It is revealed that sulfurization of MoO_3 in the plasma is affected by T_{sn}. The sulfurization process occurs in two steps, involving the reduction of MoO_3 to form MoO_2 in the first step, followed by MoO_2 being converted into MoS_2. It is also evident that the reduction of MoO_3 is more a result of the reactive species of hydrogen (H^*) than the replacement of oxygen by sulfur in the second step.

Introduction

Molybdenum disulfide (MoS_2) is a layered 2D material that has attracted the attention of researchers due to its similarities to graphene and its exquisite properties, such as the band gap and large in-plane electron mobility [1]. It is composed of layers of Mo and S arranged in a hexagonal geometry with stacks of S-Mo-S. Each S-Mo-S layer is held together by weak van der Waals forces. It is characterized by lattice constants $a = 3.16$ Å and $c = 12.58$ Å. There are many applications of MoS_2 nanostructures in the fields of tribology [2], electrochemical biosensing [3], energy storage [4, 5] and electronics [6–8]. Besides these applications, MoS_2 nanostructures have found uses in intercalation chemistry [9], sensors [10], etc.

Various techniques have been used for the synthesis of MoS_2 and reaction mechanisms have been proposed based on these experimental results. For example, Tenne *et al* [11] synthesized nested fullerene-like structures of MoS_2 by sulfurizing MoO_3 using sulfur/H_2S and reported that MoO_3 is first converted into amorphous MoS_3, which was further annealed at high temperature (850–1050 °C) to produce crystalline 2H-MoS_2. Feldman *et al* [12] gave a model for the conversion of MoO_3 into MoS_2: first MoO_3 is slowly reduced to MoO_{3-x} by H_2/N_2 (5%/95%) gas. Afterwards the suboxide was converted into MoO_2 and subsequently the oxide core is converted into sulfide. When the sulfurization of MoO_3 particles was carried out by Jong *et al* [13] using 10% H_2S in H_2 it was shown that the process of sulfurization was progressed by the involvement of oxysulfidic Mo species and Mo (IV) oxide in intermediate sulfurization stages and they also proposed the formation of hydrogen molybdenum bronze, H_xMoO_3 with $x \leqslant 2$ at low temperature. Similarly, Weber *et al* [14] showed the formation of oxysulfides at low temperatures when the sulfurization of MoO_3 was done in the presence of H_2S gas and obtained crystalline MoS_2 at higher temperature of about 800 °C. Li *et al* [15] synthesized MoS_2 nanoflowers and

nanotubes by the reaction of $MoCl_5$ and sulfur. They also reported that the sulfurization reaction is stepwise; first $MoCl_5$ is reduced and partially sulfurized forming the intermediate product MoS_xCl_y at low temperature. This group also reported that MoS_2 had a rhombohedral structure at 550 °C and a hexagonal structure at 850 °C.

Most of the reaction mechanism involves the reduction of MoO_3 and the subsequent formation of MoS_2 with an intermediate product that is favourable for the formation of the final product MoS_2. This intermediate product depends on the precursor and process used in the synthesis. The processes mentioned so far required synthesis temperatures higher than 500 °C to synthesize MoS_2. High temperature provides a high degree of crystallinity and reduces the defects in the synthesized material. However, it greatly limits the choice of substrates. The techniques that require low temperatures need additional annealing to improve the crystallinity. Techniques based on sulfur as the precursor require exposure to elemental sulfur as it sublimes in the form of a dimer (S_2) and an oligomer (S_8) [16], making it difficult to achieve control over the amount of sulfur available for the sulfurization process. The use of H_2S allows control over the sulfur content in the reaction process and simultaneously provides a reducing environment. However, the thermal decomposition of H_2S takes place above 800 °C and the thermal dissociation of H_2 takes place above 2000 °C [17].

In this work, we present plasma-assisted sulfurization (PAS) for the synthesis of MoS_2 from MoO_2 and an H_2S plasma as a function of temperature. A detailed mechanism for the sulfurization in a plasma environment is proposed in this paper based on experimental results. It was found that the reduction rate of MoO_3 is faster than its sulfurization rate in presence of the plasma. The depth of penetration of the hydrogen species is also greater than the sulfur species. The sulfurization process reveals the formation of core–shell structures at temperatures as low as 350 °C with excellent crystallinity, thereby eliminating the requirement for additional treatment steps as mentioned above. The H_2S plasma provides the reducing environment as well as the source of the sulfur species for sulfurization and releases harmless products, making this an environmentally friendly process. The advantages of using plasma are threefold. First the synthesis temperature is reduced due to the presence of the ionic species of sulfur in the plasma. Second there is a significant decline in the duration of the reaction required to convert MoO_3 into MoS_2. Third, as reduced temperatures are involved in the synthesis process, a greater range of substrates can be used.

Experiment

Plasma-assisted sulfurization of MoO_3 NTFs is achieved by treatment with an H_2S/Ar plasma. First, MoO_3 nanoflakes are deposited on a glass substrate using a plasma-assisted sublimation process (PASP) [18, 19]. These films are then placed in vacuum chamber over a molybdenum metal strip. The chamber is evacuated until the pressure inside drops down to 8.5×10^{-6} Torr. The Mo strip is then gradually heated by passing a controlled current through it until it reaches the desired temperature. The temperature is monitored by a thermocouple arrangement as shown in figure 1. Afterwards a mixture of H_2S (10%) and Ar (90%) gases is introduced into the chamber. The plasma is generated using aluminium electrodes kept at a spatial separation of 7.5 cm and a plasma voltage of 1000 V at a partial pressure of 6.5×10^{-1} Torr. The samples are treated with the H_2S/Ar plasma at 150, 250, 350, 450 and 550 °C and are abbreviated as M1, M2, M3, M4 and M5, respectively. The sulfurization process continues for 60 min, and the samples are then allowed to cool in an Ar atmosphere at a pressure of 9.0×10^{-1} Torr.

The surface morphology of all of the films is studied with SEM (ZEISS EVO series model EVO-50). Structural studies are carried out using a Rigaku Ultima IV model x-ray diffractometer equipped with Cu $K\alpha$ radiation ($\lambda \sim 1.54$ Å) source with a constant glancing angle of 1°. The 2θ range used in the measurement was from 10° to 70° in steps of 0.05°. Vibrational studies of the sulfurized films were carried out by Raman spectroscopy, using a Horiba Lab RAM HR Evolution equipped with a 514 nm Ar ion laser at 20 mW power. Transmission electron microscopy (TEM) and high-resolution TEM (HRTEM) studies were undertaken using a Tecnai F30, FE operated at 200 kV with selected area electron diffraction (SAED) analysis. Photoelectron spectroscopic studies were carried out by SPECS, with anode Mg/Al 25 kV x-ray source and a hemispherical analyser PHOIBOS HSA3500 150 R6 [HW Type 30:14] MCD-9. Measurements were taken at a pass energy of 40 eV. Charging was corrected for by using the carbon peak at 284.6 eV as a reference.

Results

XRD analysis

To study the structural changes occurring in the MoO_3 crystal structure in the presence of reactive species of the H_2S/Ar plasma at different temperatures x-ray diffraction patterns were recorded. An x-ray diffractogram (XRD) of an MoO_3 NTF is shown in figure 2 (M0). Peaks are present at 2θ value of 12.67°, 23.39°, 25.64°, 27.34°, 33.72°, 39.07°, 45.83° and 49.23°, corresponding to the (020), (110), (120), (021), (111), (060), (200) and (002)

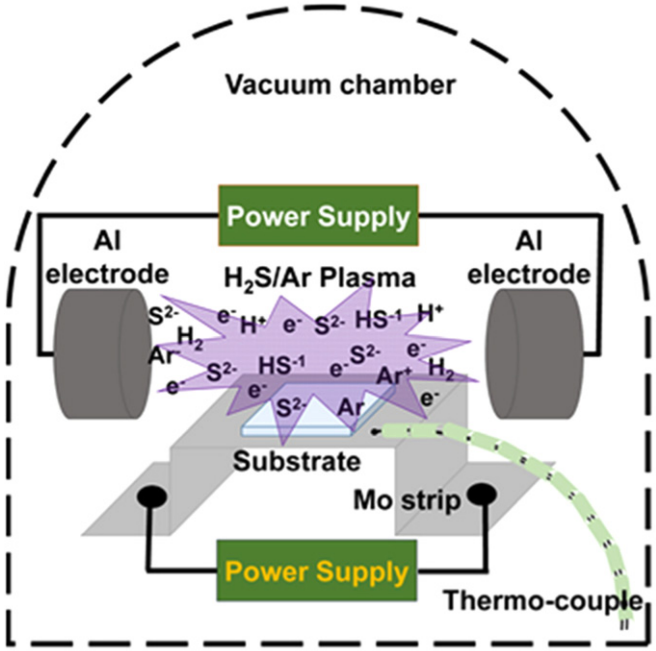

Figure 1. Schematic of plasma-assisted sulfurization set-up.

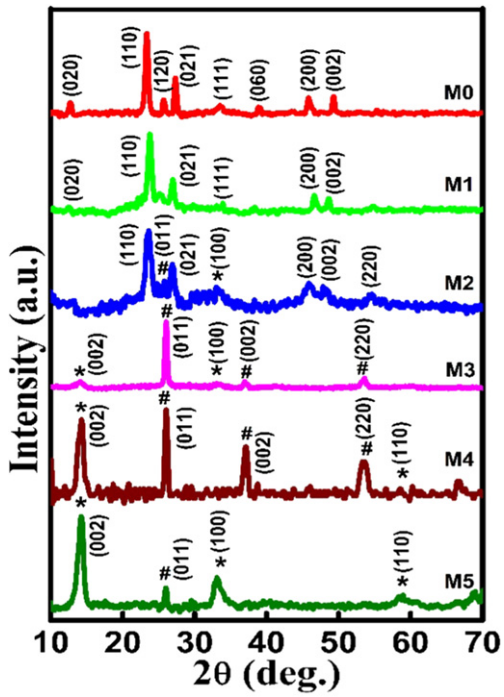

Figure 2. X-ray diffraction pattern of MoO_3 and sulfurized MoO_3 films at 150 °C (M1), 250 °C (M2), 350 °C (M3), 450 °C (M4) and 550 °C (M5). XRD peaks marked by (#) and (*) correspond to MoO_2 and MoS_2, respectively.

planes, respectively. On comparison with the reported values in JCPDS card no. 89-5108, it is confirmed that MoO_3 is present in the orthorhombic phase. The following observations are made from XRD patterns of samples M1-M5 (shown in figure 2). In M1, peaks corresponding to planes (020), (110), (021), (111), (200) and (002) are reduced in intensity with an increase in peak broadening, which implies a reduction in crystalline MoO_3 in comparison with M0. The peaks corresponding to crystal planes (120) and (060) have disappeared. Similarly, the reduction in the intensity of the peaks continued in M2 along with increased broadening and the

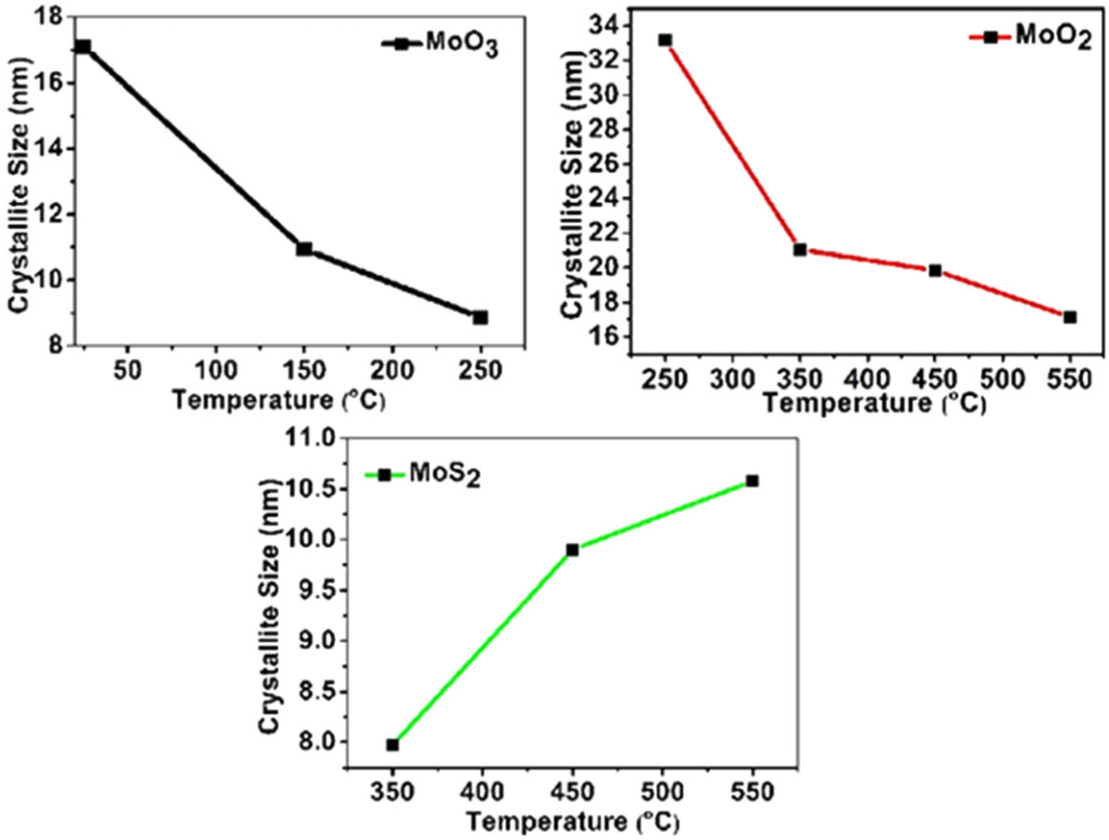

Figure 3. Average crystallite size calculated using Scherrer's equation as a function of temperature.

peaks corresponding to the (020) and (111) planes have vanished completely. The background appears to indicate content in the sample.

In M2 two new peaks are observed at 2θ values of 25.99° and 33.16°, corresponding to the (011) crystal plane of MoO_2 (marked by # in figure 2 according to JCPDS card no.78-1073) and the (002) crystal plane of MoS_2 (marked by * in figure 2 according to JCPDS card no. 37-1492) respectively. In M3, peaks relating to hexagonal phase of MoS_2 appeared at 2θ values of 14.23° and 33.16°, corresponding to the (002) and (100) planes. Similarly, peaks of monoclinic MoO_2 appeared at 2θ values of 25.99°, 37.12° and 53.67° corresponding to the (011), (002) and (220) crystal planes. The relative intensity of plane (011) of MoO_2 is higher than the (002) plane of MoS_2. No peak related to MoO_3 is observed in the XRD pattern of M3. It is therefore inferred that either MoO_3 is not present in the sample or its presence is in an amorphous form not observable by XRD. As the pattern shows the crystalline nature of the sample, the presence of crystalline MoO_3 can be eliminated. In M4, the intensity of the (002) plane of MoS_2 increased and became equal to that of the (011) plane of MoO_2. The sharp and intense peak shows an increase in crystallinity. In M5, there is increase in the intensity of the (002) plane of MoS_2. The intensity of the peak corresponding to the (011) plane of MoO_2 is reduced, whereas the (002) and (220) crystal planes have vanished.

Figure 3 shows the change in the size of the crystallites of MoO_3, MoO_2 and MoS_2 at different sulfurization temperatures. The crystallite size was calculated from the most intense peak in the XRD spectra using Scherrer's equation. First, the MoO_3 crystallite size decreases with an increase in T_{sn}. It is therefore clear that the MoO_3 grains are decreasing in size as temperature increases, further confirming that MoO_3 is present in lower quantities. Similarly, the MoO_2 crystallite size decreases, from which it can be deduced that the presence of MoO_2 is diminishing as T_{sn} increases. Contrary to MoO_3 and MoO_2, the crystallite size of MoS_2 increases with T_{sn}. Thus it can be inferred that the presence of MoS_2 is more pronounced at higher temperatures.

From these results it can be observed that at a sulfurization temperature of 150 °C disorder begins to set in, which is observed between 2θ value of 15° and 30° (M1). It must be noted that the (120) crystal plane of MoO_3 was the first to disappear completely. As T_{sn} is increased to 250 °C, this disorder has clearly spread throughout the crystal, indicating the partial collapse of the lattice structure of MoO_3, which is evident from the broadening of the peaks. However, the crystal structure is not completely destroyed yet; a slight degree of rearrangement associated with the formation of MoO_2 has been initiated as shown by the appearance of the MoO_2 peak at a 2θ

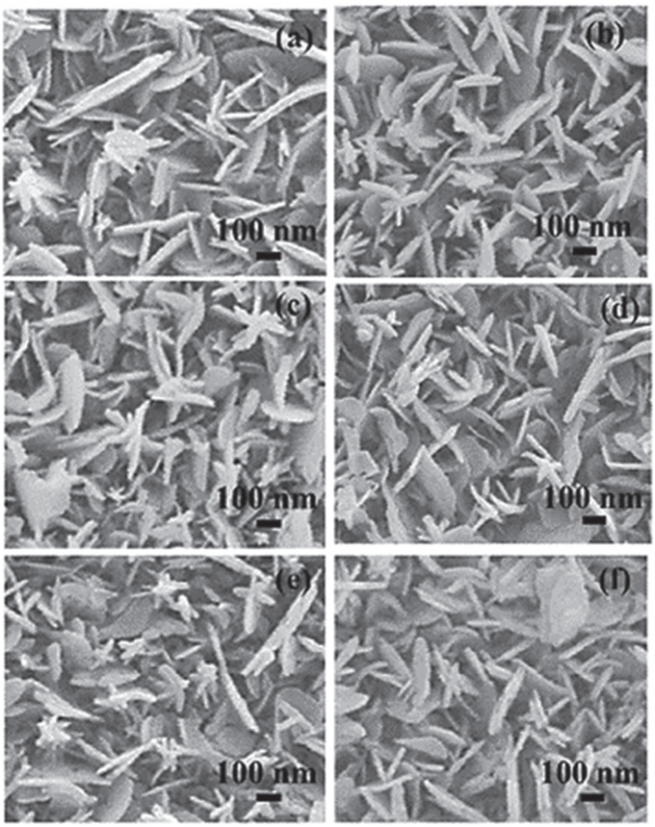

Figure 4. SEM images of the (a) as-deposited MoO_3 nanoflakes and MoO_3 sulfurized films at temperatures of (b) 150 °C, (c) 250 °C, (d) 350 °C, (e) 450 °C and (f) 550 °C.

value of 25.96°, which corresponds to the (011) crystal plane (M2). Until this stage no peaks corresponding to MoS_2 were detected, however the reduction of MoO_3 to MoO_2 is noted.

The XRD of M3 clearly shows that MoO_3 is completely reduced to MoO_2, because no peaks associated with MoO_3 are observed except for the prominent monoclinic phase of MoO_2 (marked by # in figure 2 according to JCPDS card no.78-1073), which appeared with the most intense peak at a 2θ value of 25.96°, along with a peak for MoS_2 (marked by * in figure 2 according to JCPDS card no. 37-1492) at a 2θ value of 14.28°. It is hereby inferred that the crystal structure has reorganized to form MoO_2 and the sulfurization of MoO_2 to form MoS_2 by replacing oxygen with sulfur has taken place. The XRD pattern of films sulfurized at 450 °C shows a decrease in the intensity of the peaks that correspond to MoO_2. The intensity of peak corresponding to crystal plane (002) at a 2θ value of 14.28° becomes higher, confirming that the MoS_2 phase is strengthened. At 550 °C (M5), conversion of MoO_2 into hexagonal MoS_2 is almost complete, as indicated by the peaks at 2θ values of 14.28°, 33.45° and 58.76°, along with the minor amount of MoO_2.

SEM analysis

Figure 4(a) presents the SEM image of the as-deposited MoO_3 film, which was grown on a glass substrate, clearly showing the oriented and aligned growth of the MoO_3 nanoflakes. The average width of the nanoflakes ranges from 100 nm to 400 nm. Figures 4(b)–(f) shows the SEM images of sulfurized samples M1, M2, M3, M4 and M5, respectively. There is no noticeable difference in the morphology before and after the sulfurization of the films.

Raman analysis

Studying the vibrations in the samples provided further insight into the process taking place at the structural level. For this purpose, Raman spectra of the samples were recorded. The Raman spectrum of the as-deposited MoO_3 film is shown in figure 5 (M0). Analysis of the MoO_3 spectrum shows that all of the vibrational peaks positioned at 244, 287, 336, 664, 820 and 993 cm^{-1} are in good agreement with those reported for α-MoO_3 [18]. These sharp and intense peaks indicate a good degree of crystallinity in the MoO_3 film. The peaks at 664, 820 and 993 cm^{-1} are due to the Mo-O stretching modes occurring from the triply coordinated oxygen (Mo-O_3), doubly coordinated oxygen (Mo-O_2) and the terminal oxygen (Mo-O_1), respectively. The peaks at 244, 287 and

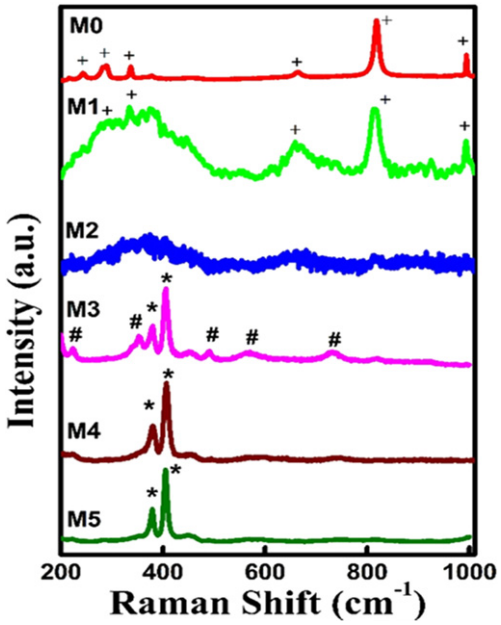

Figure 5. Raman spectra of MoO_3 (M0) and sulfurized MoO_3 films at temperatures of 150 °C (M1), 250 °C (M2), 350 °C (M3), 450 °C (M4) and 550 °C (M5). Characteristic peaks are marked by: MoO_3(+), MoO_2(#) and MoS_2 (*).

338 cm^{-1} are due to the bending modes of MoO_3. At 150 °C, the peaks associated with MoO_3 are not only reduced but also broadened. This shows that crystallinity of MoO_3 is reduced.

In the Raman spectrum of M2, the loss of crystallinity in the MoO_3 film is evidenced by the absence of sharp and intense peaks due to MoO_3. The characteristic peaks corresponding to MoS_2 at 379 cm^{-1} (the in-plane vibration of Mo-S) and 405 cm^{-1} (the out-of-plane vibration of the S atoms) [2, 20, 21] are observed in M3. In addition to these two peaks, the peaks positioned at 224, 354, 490, 571 and 731 cm^{-1} are also recorded, corresponding to the monoclinic MoO_2 phase [22]. Hence it is concluded that the crystal structure is reorganized after an amorphous phase (figure 5 (M3)). This has also been confirmed previously by XRD results. As T_{sn} is increased to 450 °C, all of the peaks associated to MoO_2 disappear and the intensity of the MoS_2 peaks increases, which indicates that the surfaces of the nanoflakes have been converted into MoS_2. This is further supported by the HRTEM results (discussed in a later section). The intensity and sharpness of the MoS_2 peaks is enhanced with increasing T_{sn} to 550 °C. Therefore, the Raman analysis supports the surface of the MoO_3 film being completely converted into MoS_2 and these results are well corroborated by the XRD findings for samples M1M5.

XPS analysis

X-ray photoelectron spectra of the MoO_3 film and the films sulfurized at different temperatures are shown in figures 6(a)–(f). Table 1 shows the relative changes in the positions of the binding energies and the relative percentages of Mo oxidation (for the 6+ and 4+) states calculated using the best-fitted Gaussian curves that correspond to the peaks of Mo 3*d*. All of the data are calibrated with the C (1s) peak, which was recorded at constant binding energy of 284.6 ± 0.2 eV in all of the samples. Figure 6(a) shows the MoO_3 spectrum with an Mo 3*d* doublet corresponding to Mo $3d_{5/2}$ at a binding energy of 232.45 eV and $3d_{3/2}$ at a binding energy of 235.38 eV, which is characteristic of molybdenum in a 6^+ oxidation state [23]. As shown in the spectra, after sulfurization there are three components of molybdenum: first MoO_3 at 232.18 eV, second MoO_2 at 229.26 eV and third MoS_2 at 228.68 eV [24]. As the peaks of MoO_2 overlap with those of MoS_2 it is difficult to identify the relative content of both of these phases using the Mo 3*d* doublet.

There are in general two methodologies for finding the relative composition of a material [24]. The first uses the S/Mo ratio from survey scan plots, for example at 350 °C in figure 6 the S/Mo ratio is 1.54 and the calculated relative content of MoS_2 thus is 77%, using the standard value of S/Mo = 2. In the second method, the MoS_2 content is calculated by deconvoluting the peak that is evaluated to be 74.5%, which is in good agreement with values obtained from previously calculated values.

For the sample sulfurized at 150 °C, two molybdenum oxidation states are present. No peak corresponding to sulfur is observed but a relative shift in the binding energy of Mo is recorded towards a lower binding energy, implying that the film surface has been reduced to MoO_2. This is confirmed by the Raman analysis. The Mo $3d_{5/2}$

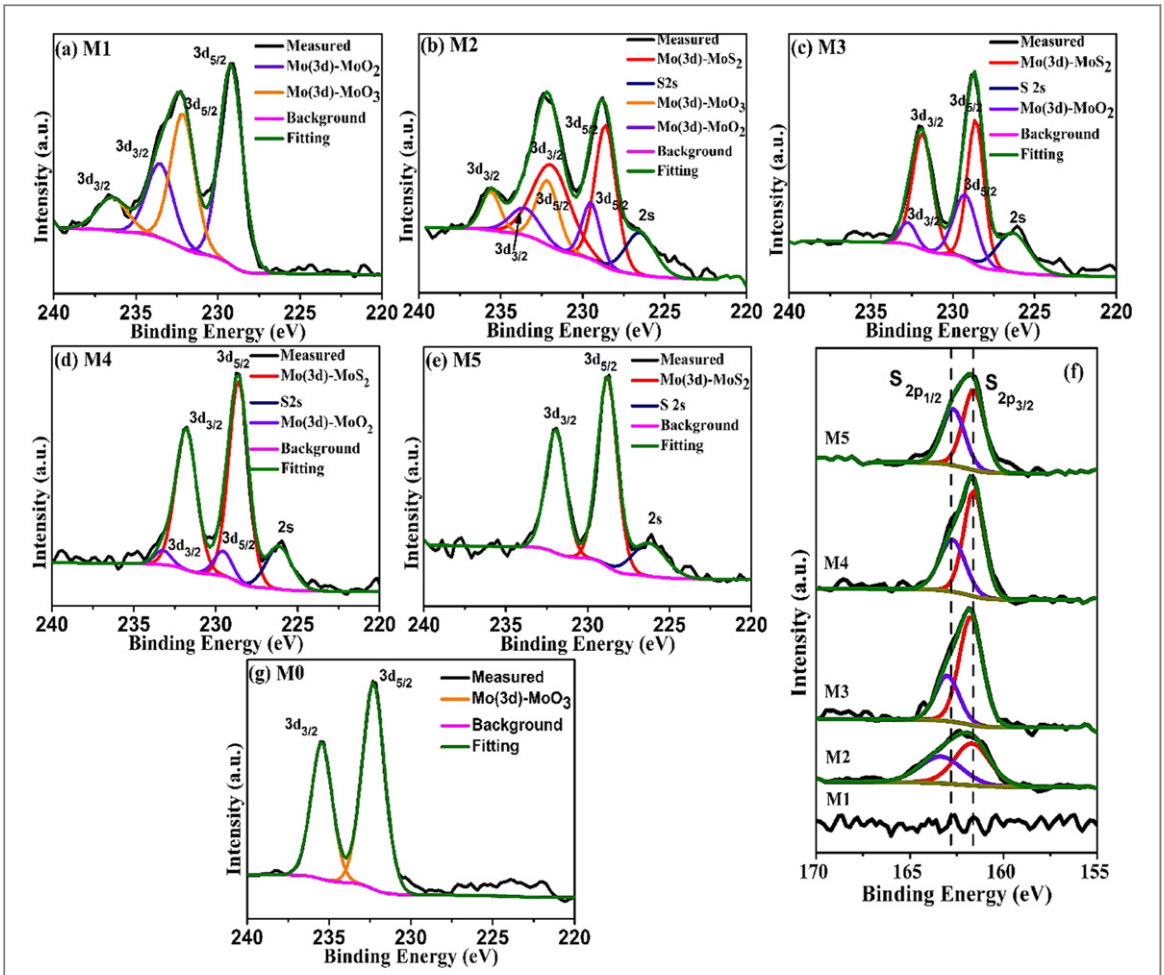

Figure 6. X-ray photoelectron spectra of sulfurized MoO_3 films at temperatures of (a) 150 °C (M1), (b) 250 °C (M2), (c) 350 °C (M3), (d) 450 °C (M4) and (e) 550 °C (M5); (f) core scan of the S 2*p* doublet peaks and (g) MoO_3.

Table 1. Summary of the XPS analysis. The peak position and related shift in the Mo 3*d* binding energy after sulfurization for the MoO_3 films and the relative change in the percentages of MoO_3, MoO_2 and MoS_2 for different temperatures.

		Mo^{6+} (MoO_3)		Mo^{4+} (MoO_2)		Mo^{4+} (MoS_2)	
Temp. (°C)	S/Mo	Position (eV)	Relative content (%)	Position (eV)	Relative content (%)	Position (eV)	Relative content (%)
MoO_3	—	232.30	100	—	—		—
150	—	232.18	60.78	229.26	39.36	—	—
250	1.36	232.12	21.1	229.46	12.5	228.68	66.8
350	1.54	—	—	229.29	25.5	228.62	74.5
450	1.86	—	—	229.50	7.7	228.63	92.3
550	1.98	—	—		1.5	228.79	98.5

peak is fitted to the two peaks positioned at 232.18 eV and 235.40 eV, corresponding to Mo^{6+} oxidation state. The doublet peaks at 229.26 eV and 232.37 eV belong to Mo^{4+} and the relative contents of MoO_3 and MoO_2 are 60.78% and 39.36% respectively. This indicates that the Mo^{6+} content has been reduced by 39.22%.

When T_{sn} is 250 °C, the relative percentage of the MoO_3 phase is decreased by 79.9% (compared with the actual content of MoO_3) and the doublet peaks of MoS_2 with the Mo4+ oxidation state appeared at 228.68 eV and 234.68 eV, with MoO_2 doublet peaks at 229.46 eV and 231.85 eV [13]. It is therefore confirmed that the film is composed of three components (i.e. MoO_3, MoS_2 and MoO_2) and their relative percentages are 21.1%, 66.8% and 12.5, respectively. It is inferred that top-most layers of the nanoflakes have been sulfurized to form MoS_2.

With a further increase in T_{sn} to 350 °C, a smaller degree of change can be seen in the positions of the binding energies of the Mo 3*d* peaks corresponding to the MoS_2 and MoO_2 oxidation states of Mo. But the contents of MoO_2 has increased from 12.5% to 25.5% because the reduction of MoO_3 to MoO_2 in the presence of the

plasma is much faster than the sulfurization of MoO_2 into the MoS_2 phase. This is because in the H_2S plasma the relative concentrations of the H ionic species are higher than sulfur ions. In addition, the smaller size of the hydrogen atoms also means they diffuse into the nanoflakes more readily thus enabling them to reach the core of the nanostructure and reduce it at a much faster rate than sulfur. This is supported by the relative increment of MoS_2 from 66.8% to 74.5%, which is much lower than the relative increment of MoO_2. As T_{sn} is increased from 350 °C to 550 °C no change in the peak positions of MoO_2 and MoS_2 took place. However, changes in the relative percentages of both the phases were found. MoS_2 has increased significantly almost to 99%, whereas MoO_2 almost disappears.

This increment in MoS_2 at higher temperature is due to the fact that more and more of the sulfur species diffuses into the core and thereby replace the oxygen with sulfur and form MoS_2. Figure 6(f) displays the S 2*p* spectrum, which shows a doublet of S $2p_{3/2}$ at 161.4 eV and S $2p_{1/2}$ at 162.9 eV [20]. Examination of the S 2*p* peak shows that sulfur is present in the S^{2-} oxidation state, confirming the formation of MoS_2. The presence of elemental sulfur has not been found as no peaks appeared at 164.1 eV. The absence of a sulfur peak at 150 °C shows that the surface of the nanoflake has been reduced. With increasing T_{sn} the peaks corresponding to sulfur appear, but its spectra at 250 °C is broader than those obtained after sulfurization at higher temperatures. The broadening of the peak can be attributed to the various sulfur species. The first of these is the thiomolybdate species, with a binding energy in the range of 162.3–163.5 eV. These structures have core of Mo_xS_y [25], ($x \neq y >$ 1) and the formation of these species is related to the anion vacancies in the MoS_2 lattice where the S/Mo ratio is near unity. Another is due to the presence of sulfhydryl groups [26] (SH^-) with a binding energy in the range of 161.9 eV–164.2 eV. As T_{sn} increases this broadening disappears from the spectra of sulfur.

HRTEM studies

The samples for TEM measurements were prepared by suspending nanoflakes from the MoO_3 film and sulfurized films in ethanol (C_2H_5OH). After prolonged ultrasonication a few drops of the well-dispersed solution were put onto the standard carbon-supported 600 mesh copper grid and dried slowly at room temperature. Figure 7(a) shows the bright-field TEM micrograph of an MoO_3 nanoflake, confirming that the NFs have a large surface area and well-defined dimensions with an average width of 200 nm. These dimensional analyses are consistent with the SEM results. Figures 7(b) and (c) shows the TEM micrographs of an MoO_3 film sulfurized at 350 °C at low and high magnifications, respectively. The recorded TEM micrograph at high magnification from the outer surface of NF shows that the *d*-spacing between two adjacent layers is 0.634 nm, which is in good agreement with the *d*-spacing of the MoS_2 (002) crystal plane as reported in literature [27]. Figure 7(c) shows 3-4 monolayers of MoS_2. TEM micrographs of a film sulfurized at 450 °C (figure 7(d)) support the core–shell structure of the nanoflakes. The results show that the diffusion of the S species increases as the thickness of the layered MoS_2 increased to 9-15 monolayers. The core of a single nanoflake is further analysed by HRTEM (micrograph shown in figure 7(e)). At the core, the recorded fringe pattern shows the (011) crystal plane of MoO_2 with a lattice spacing of 0.338 nm [28], which is confirmed by the results obtained from XRD patterns where the monoclinic phase of MoO_2 is present.

It is thus confirmed that MoO_3 is first reduced to MoO_2 and then converted to MoS_2. As the temperature is increased to 550 °C, the MoS_2 layered structure seems to penetrate deeper to the core of the nanoflakes; figures 7(g) and (h) show that the number of monolayers of MoS_2 has increased to $\geqslant$30.

Discussion

Molybdenum trioxide is transition metal oxide with a layered structure composed of corner-shared and edge-shared MoO_6 octahedra, as shown in figure 8. Every MoO_6 octahedra has an Mo metal atom at the centre with one single-shared oxygen atom (shown in violet), two doubly shared oxygen atoms (green) and three triply shared oxygen atoms (red) [29]. The sulfurization of MoO_3 can now be explained as a two-step process. In the first step, MoO_3 is reduced in the presence of a hydrogen sulfide plasma to MoO_2. In the second step, MoO_2 is converted to MoS_2 by the replacement of oxygen with sulfur. In order to better understand the processes behind the sulfurization, a closer look at the intermediate steps is essential. These steps are summarized as chemical reactions (1) and (3). Reaction (2) is the detailed representation of (1) in presence of ionic species, as would be the case where the plasma is involved. Similarly, reactions (4) and (5) are detailed reactions written for reaction (3).

Step 1:

$$MoO_3 + H_2 \rightarrow MoO_2 + H_2O \quad (1)$$

$$MoO_3 + 2H^+ + 2e^- \rightarrow MoO_2 + H_2O \quad (2)$$

Step 2:

$$MoO_2 + 2H_2S \rightarrow MoS_2 + 2H_2O \quad (3)$$

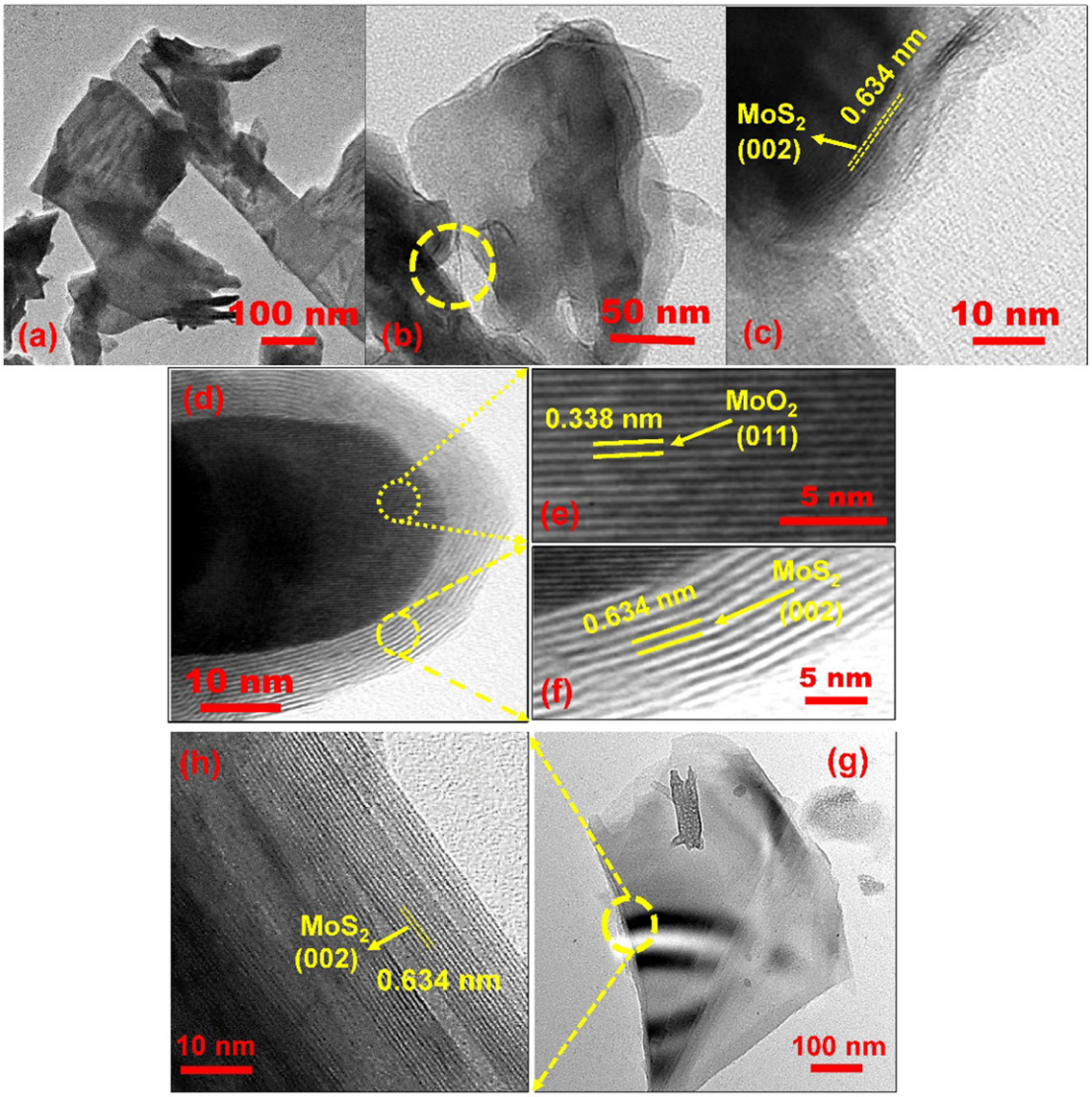

Figure 7. HRTEM micrograph of (a) an MoO_3 NTF, (b)–(c) sulfurized film at 350 °C, (d) sulfurized film at 450 °C, (e) MoO_2 core seen at 5 nm scale, (f) MoS_2 shell layers seen at 5 nm scale, (g) sulfurized film at 550 °C and (h) high-resolution image recorded from the encircled region in (g).

$$MoO_2 + 2HS^{-1} + 2H^+ \rightarrow MoS_2 + 2H_2O \quad (4)$$

$$MoO_2 + 2S^{2-} + 4H^+ \rightarrow MoS_2 + 2H_2O \quad (5)$$

The mere presence of reactants at a certain temperature does not necessarily result in the formation of products. For any reaction to be feasible, the Gibbs free energy change (ΔG) for that reaction must be negative. A negative energy implies that the reaction is forward and that the reactants will react to form products. The ΔG values reported by Kadiev *et al* [17] for reaction (1) at temperatures of 300, 400 and 500 °C are −79.749, −72.961 and −67.004 KJ mol^{-1} respectively, and for reaction (3), ΔG is −120.262, −118.697 and −117.060 KJ mol^{-1} at the same temperatures. It is clear that reactions (1) and (3) are favourable. Hence, the formation of MoO_2 and MoS_2 is unequivocal. The first step in sulfurization is the reduction of MoO_3 to MoO_2 in the reducing environment of an H_2S plasma. It is known that the plasma consists of ionized species of the gas. The reduction potential of hydrogen is 0 V as hydrogen acts as a standard electrode while measuring the reducing capabilities of other reducing/oxidizing agents. H_2S is reductant, with a reduction potential of almost 0.14 V.

This means that H_2S provides a slightly less reducing environment than H_2, but the presence of atomic sulfur (which is created by the dissociation of the H_2S gas in a plasma) is very much reducing compared with H_2S, with the reduction potential of atomic S nearly −0.48 V, greater than that of H_2S. This implies that the atomic and ionic species of hydrogen and sulfur are more reducing than H_2S itself. However, as the plasma is used many ionic species are present, which creates a niche suitable for the reduction of MoO_3 by hydrogen ions. This reduction is detected in the XRD analysis, as the peaks that correspond to MoO_3 decrease in intensity and

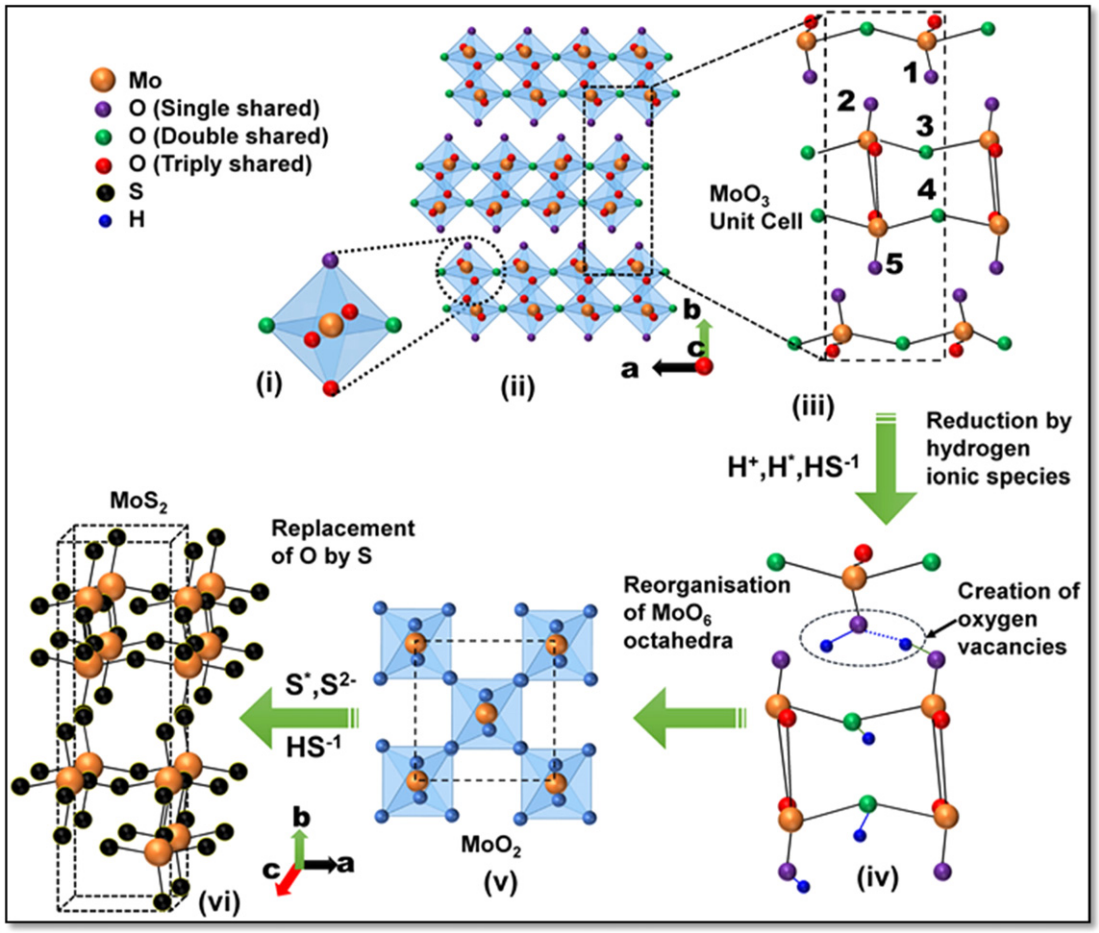

Figure 8. Schematic representation of the sulfurization of MoO_3 to MoS_2.

eventually disappear. MoO_2 simultaneously starts to appear as T_{sn} increases from 150 °C to 250 °C. The Raman spectra of M1 and M2 also depict the peaks that correspond to the vibrations of MoO_3 reducing in intensity and disappearing as T_{sn} is increased, thus supporting the results obtained by XRD. The reduction of MoO_3 is marked by the creation of oxygen vacancies [30]. Xianwei *et al* [31] have shown that the diffusion of hydrogen in MoO_3 starts with adsorption on terminal oxygen atoms and migrates towards asymmetric oxygen, continuing its migration inside the layers in a manner that requires energies of around 0.06 eV to 0.13 eV (as can be seen figure 8 (iii)). The activation energy for H diffusion is reported to be 0.1 eV–0.3 eV [32]. Hydrogen atoms, when absorbed on terminal sites, may lead to the formation of hydrogen bonds, which are stronger than the existing van der Waal's separation between the layers. This leads to the removal of oxygen from the MoO_3 crystal in the form of H_2O, resulting in the formation of an oxygen vacancy and the slightly non-stoichiometric oxide MoO_{3-x} [33–35]. At low temperatures, oxygen vacancies are ordered and do not affect the layered structure of MoO_3 as shown in the XRD patterns of M1 and M2, where peaks related to the MoO_3 structure are present at 2θ value of 23.33°, 27.298° and 33.739°. However, at higher temperatures, these vacancies appear to aggregate on the (120) crystallographic planes in MoO_3, which collapse to form a shear plane in order to eliminate vacancies. The formation of shear results in the disappearance of the (120) plane of MoO_3, as observed in the XRD pattern of M2 at $T_{sn} = 250$ °C. Further increases in shear planes leads to the collapse of the layered crystal structure and the reorganization of the MoO_6 octahedra [30]. This led to the formation of MoO_2, as detected in the XRD pattern and Raman spectra of M3. Interestingly, at 350 °C simultaneous sulfurization is taking place, and is recorded in both XRD patterns and Raman spectra. The next step in sulfurization is the conversion of MoO_2 into MoS_2. This is achieved by the direct replacement of oxygen by sulfur as per reactions (4) and (5). The results obtained from XRD and Raman analysis show the presence of both MoO_2 and MoS_2 in M3 and M4, supported by HRTEM, which shows an MoO_2/MoS_2 core–shell-like structure. MoO_2 forms the unreacted core, whereas the surface has the signature of MoS_2. As T_{sn} is increased, so does the depth at which MoO_2 is converted to MoS_2. These results are also supported by Raman and XRD analysis, and are seen in figures 7(c)–(f) (HRTEM). At an even higher temperature of sulfurization (550 °C), the MoO_2 core is perceived to be converted into MoS_2. So far , the results support each other in the initial stages of sulfurization. For a better understanding of the sulfurization process,

various models have been adopted. In most cases concerning diffusion Fick's law of diffusion is applied. However, in the case of sulfurization, the diffusion of sulfur is better understood by the Deal Grove model [36]. First, the top layers of MoO_2 were converted into MoS_2, after that sulfurization is limited by the rate of diffusion of the sulfur species through the already formed MoS_2 layered structure. The conversion reaction between MoO_2 and the sulfur species takes place at the interface of MoO_2 and MoS_2. As the size of elemental sulfur (~100 pm) is smaller than that of the H_2S molecule (~390 pm), it is easier for S species to diffuse into the MoS_2 layers than H_2S molecules. It is therefore concluded that the presence of the H_2S plasma not only provides reactive species but also lowers the energy required for the reaction to take place, thereby reducing the temperature at which sulfurization takes place—as is observed in the obtained results.

Conclusions

In summary, plasma-assisted sulfurization of MoO_3 NTFs has been carried out and the mechanism behind the conversion of MoO_3 into MoS_2 in the presence of reactive species of H_2S/Ar (H^+, S^*, S^{2-}, etc) in plasma has been studied. Sulfurization of MoO_3 films is accomplished at five different temperatures from 150 °C to 550 °C in steps of 100 °C. It has been found out that the mechanism behind the formation of MoS_2 from MoO_3 is understood as a two-step process. First involving reduction of precursor MoO_3 into MoO_2 followed by replacement of oxygen by sulfur in MoO_2 to form MoS_2. The rate of reduction is higher than the rate of replacement of oxygen by sulfur. Sulfurized films have been studied with SEM, XRD, Raman, XPS and HRTEM techniques. The obtained results show that sulfurization is initiated at temperatures as low as 350 °C and higher temperatures result in increments in MoS_2. For sulfurization temperatures $\leqslant$350 °C, there is distortion of the MoO_3 crystal structure due to the reducing environment created by ionic species of H and S, which further resulted in the formation of monoclinic MoO_2 because of the reorganization of the crystal structure. At higher temperatures the replacement of O by S yields MoS_2.

Acknowledgments

We thankfully acknowledge the use of Ultima IV Rigaku x-ray Diffractometer and Raman spectrometer facility at the Nanoscale Research Facility and the use of XPS (partially funded by an FIST grant of the DST) and HRTEM at the Indian Institute of Technology Delhi.

References

[1] Li H, Qi X, Wu J, Zeng Z, Wei J and Zhang H 2013 Investigation of MoS_2 and graphene nanosheets by magnetic force microscopy *ACS Nano* **7** 2842–9
[2] Windom B C, Sawyer W G and Hahn D W 2011 A raman spectroscopic study of MoS_2 and MoO_3: applications to tribological systems *Tribol. Lett.* **42** 301–10
[3] Kim H-U, Kim H, Ahn C, Kulkarni A, Jeon M, Yeom G Y, Lee M-H and Kim T 2015 *In situ* synthesis of MoS_2 on a polymer based gold electrode platform and its application in electrochemical biosensing *RSC Adv.* **5** 10134–8
[4] Zhang X, Liang J and Ding S 2014 The application of nanostructure MoS_2 materials in energy storage and conversion MoS_2 (*Lecture Notes in Nanoscale Science and Technology* vol 21) ed Z M Wang (Berlin: Springer) pp 237–68
[5] Huffstutler J D 2014 An analysis of electrochemical energy storage using electrodes fabricated from atomically thin 2D structures of MoS_2, graphene and MoS_2/graphene composites *MSc Thesis* Southern Illinois University, Carondale
[6] Cheng R, Jiang S, Chen Y, Liu Y, Weiss N, Cheng H-C, Wu H, Huang Y and Duan X 2014 Few-layer molybdenum disulfide transistors and circuits for high-speed flexible electronics *Nat. Commun.* **5** 5143
[7] Espinosa F M, Ryu Y K, Marinov K, Dumcenco D, Kis A and Garcia R 2015 Direct fabrication of thin layer MoS_2 field-effect nanoscale transistors by oxidation scanning probe lithography *Appl. Phys. Lett.* **106** 103503
[8] Li H-M, Lee D, Qu D, Liu X, Ryu J, Seabaugh A and Yoo W J 2015 Ultimate thin vertical p–n junction composed of two-dimensional layered molybdenum disulfide *Nat. Commun.* **6** 6564
[9] Woollam J A and Somoano R B 1977 Physics and chemistry of MoS_2 intercalation compounds *Mater. Sci. Eng.* **31** 289–95
[10] Kalantar-zadeh K and Ou J Z 2016 Biosensors based on two-dimensional MoS_2 *ACS Sensors* **1** 5–16
[11] Margulis L, Salitra G, Tenne R and Talianker M 1993 Nested fullerene-like structures *Nature* **365** 113–4
[12] Feldman Y, Frey G L, Homyonfer M, Lyakhovitskaya V, Margulis L, Cohen H, Hodes G, Hutchison J L and Tenne R 1996 Bulk synthesis of inorganic fullerene-like MS_2 (M = Mo, W) from the respective trioxides and the reaction mechanism *J. Am. Chem. Soc.* **118** 5362–7
[13] de Jong A M, Borg H J, van IJzendoorn L J, Soudant V G F M, de Beer V H J, van Veen J A R and Niemantsverdriet J W 1993 Sulfidation mechanism by molybdenum catalysts supported on silica/silicon(100) model support studied by surface spectroscopy *J. Phys. Chem.* **97** 6477–83
[14] Weber T, Muijsers J C, van Wolput J H M C, Verhagen C P J and Niemantsverdriet J W 1996 Basic reaction steps in the sulfidation of crystalline MoO_3 to MoS_2, as studied by x-ray photoelectron and infrared emission spectroscopy *J. Phys. Chem.* **100** 14144–50
[15] Li X L and Li Y D 2003 Formation of MoS_2 inorganic fullerenes (IFs) by the reaction of MoO_3 nanobelts and S *Chem. Eur. J.* **9** 2726–31
[16] Morrish R, Silverstein R and Wolden C A 2012 Synthesis of stoichiometric FeS_2 through plasma-assisted sulfurization of Fe_2O_3 nanorods *J. Am. Chem. Soc.* **134** 17854–7

[17] Kadiev K M, Gyul'maliev A M, Shpirt M Y and Khadzhiev S N 2010 Thermodynamic and quantum chemical study of the transformations and operation mechanism of molybdenum catalysts under hydrogenation conditions *Pet. Chem.* **50** 312–8
[18] Sharma R K and Reddy G B 2014 Synthesis and characterization of α-MoO_3 microspheres packed with nanoflakes *J. Phys. D: Appl. Phys.* **47** 65305
[19] Sharma R K and Reddy G B 2013 Controlled growth of vertically aligned MoO_3 nanoflakes by plasma assisted paste sublimation process *J. Appl. Phys.* **114** 1–8
[20] Qin P, Fang G, Ke W, Cheng F, Zheng Q, Wan J, Lei H and Zhao X 2014 *In situ* growth of double-layer MoO_3/MoS_2 film from MoS_2 for hole-transport layers in organic solar cell *J. Mater. Chem.* A **2** 2742
[21] Li H, Zhang Q, Yap C C R, Tay B K, Edwin T H T, Olivier A and Baillargeat D 2012 From bulk to monolayer MoS_2: evolution of Raman scattering *Adv. Funct. Mater.* **22** 1385–90
[22] Camacho-López M A, Escobar-Alarcón L, Picquart M, Arroyo R, Córdoba G and Haro-Poniatowski E 2011 Micro-Raman study of the *m*-MoO_2 to α-MoO_3 transformation induced by cw-laser irradiation *Opt. Mater.* **33** 480–4
[23] Zingg D, Makovsky L, Tischer R, Brown F and Hercules D 1980 A surface spectroscopic study of molybdenum-alumina catalysts using x-ray photoelectron, ion-scattering, and Raman spectroscopies *J. Phys. Chem.* **84** 2898–906
[24] Spevack P A and McIntyre N S 1993 A Raman and XPS investigation of supported molybdenum oxide thin films: 2. Reactions with hydrogen sulfide *J. Phys. Chem.* **97** 11031–6
[25] Muller A, Jostes R, Jaegermann W and Bhattacharyya R G 1980 Spectroscopic investigations on the molecular and electronic structure of $[Mo_3S_{13}]^{2-}$, a discrete binary transition metal sulfur cluster *Inorg. Chim. Acta* **41** 259–63
[26] Srnastava S 1986 ESCA studies of metal complexes *Appl. Spectrosc. Rev.* **22** 401–535
[27] Zhou W, Hou D, Sang Y, Yao S, Zhou J, Li G, Li L, Liu H and Chen S 2014 MoO_2 nanobelts@nitrogen self-doped MoS_2 nanosheets as effective electrocatalysts for hydrogen evolution reaction *J. Mater. Chem.* A **2** 11358
[28] Zhou G, Xu X, Yu J, Feng B, Zhang Y, Hu J and Zhou Y 2014 Vertically aligned MoS_2/MoO_x heterojunction nanosheets for enhanced visible-light photocatalytic activity and photostability *Cryst. Eng. Comm.* **16** 9025–32
[29] Kalantar-zadeh K *et al* 2010 Synthesis of nanometre-thick MoO_3 sheets *Nanoscale* **2** 429–33
[30] Levy F 1976 *Crystallography and Crystal Chemistry of Materials with Layered Structures* (Dordrecht: Reidel) pp 93–125
[31] Sha X, Chen L, Cooper A C, Pez G P and Cheng H 2009 Hydrogen absorption and diffusion in bulk α-MoO_3 *J. Phys. Chem.* C **113** 11399–407
[32] Ritter C, Müller-Warmuth W and Schöllhorn R 1985 Structure and motion of hydrogen in molybdenum bronzes H_xMoO_3 as studied by nuclear magnetic resonance *J. Chem. Phys.* **83** 6130
[33] Schulmeyer W V and Ortner H M 2003 Mechanisms of hydrogen reduction of molybdenum oxides *Met. Powder Rep.* **58** 33
[34] Dang J, Zhang G-H, Chou K-C, Reddy R G, He Y and Sun Y 2013 Kinetics and mechanism of hydrogen reduction of MoO_3 to MoO_2 *Int. J. Refract. Met. Hard Mater.* **41** 216–23
[35] Choi J G and Thompson L T 1996 XPS study of as-prepared and reduced molybdenum oxides *Appl. Surf. Sci.* **93** 143–9
[36] Deal B E and Grove A S 1965 General relationship for the thermal oxidation of silicon *J. Appl. Phys.* **36** 3770–8